IEEE Access
Multidisciplinary ⋮ Rapid Review ⋮ Open Access Journal

Received September 25, 2020, accepted October 9, 2020, date of publication October 21, 2020, date of current version November 12, 2020.

Digital Object Identifier 10.1109/ACCESS.2020.3032881

An Ultra-Wide Band Radome for High-Performance and Dual-Polarized Radar and Communication Systems

ZEESHAN QAMAR[1], (Member, IEEE), JORGE L. SALAZAR-CERRENO[1,2], (Senior Member, IEEE), AND NAFATI ABOSERWAL[1,2], (Member, IEEE)

[1]Advanced Radar Research Center (ARRC), The University of Oklahoma, Norman, OK 73019, USA
[2]School of Electrical and Computer Engineering, The University of Oklahoma, Norman, OK 73019, USA

Corresponding author: Jorge L. Salazar-Cerreno (salazar@ou.edu)

This work was supported in part by the U.S. Department of Defense, Office of Naval Research (DOD-ONR), under Grant N00014-18-1-2035, and in part by the Office of Navy Research (ONR) under Grant 1532140.

ABSTRACT This paper presents a new design technique to develop a multi-layer radome for ultra-wide-band, dual-polarized radar and communication systems. In the proposed technique, a multi-layer radome is designed using a combination of A-sandwich structures, which are not used in conventional multi-layer radomes. In contrast with conventional radomes, this technique enables a substantial increase of bandwidth with a negligible change in the overall radome thickness. In addition, it provides excellent RF performance, thermal isolation, and mechanical strength. Three different multi-layer radomes for different bandwidths are designed. Parameters such as co-polarization mismatch and depolarization ratio are used to evaluate the proposed dual-polarized radome as a function of incident angle and frequency. To validate this new technique, a 5A-sandwich radome is designed to operate from 1 GHz to 14 GHz and its RF performance is evaluated by measuring S-parameters. The proposed radome is further investigated by measuring the radiation patterns of horn antennas at different bands (S-, C-, X- and Ku-bands) with and without the radomes. The measured losses recorded are below 0.5 dB with an absolute error less than 0.05 dB between the calculations and measurements. An S-band electronically scanned active phased array antenna is also used to evaluate the radome as a function of incident angles. In this case, the maximum recorded losses are below 0.4 dB and the absolute errors between the calculations and measurements are below 0.1 dB. The proposed technique and radome can be used in different applications such as surveillance systems, earth exploration satellite, aeronautical radio-navigation, and especially in dual-polarized weather radars that require a high polarization performance.

INDEX TERMS A-sandwich, dual-polarized, multi-band, multi-layer, planar, radar, radome, ultra-wide band (UWB), wideband.

I. INTRODUCTION

A radome, an acronym originates from radar dome, is a structure placed over an antenna to protect it from the environment such as wind, temperature, dust, rain, snow, etc., [1]–[6]. Ideally, the radome must pass electromagnetic waves without any degradation of electromagnetic (EM) performance of the enclosed antenna. The radome can be manufactured in the desired shape based on its application such as marines, aircraft, missiles, and other vehicles carrying the radar. Therefore, the structural integrity of the radome competes with its electromagnetic transparency and the level of competition depends on the requirements related to a particular application environment. The radome is a more critical component in weather applications where dual-polarized radar systems are implemented. Radome enables target accuracy for polarimetric radar products such as the differential reflectivity (Z_{DR}) and linear depolarization ratio (LDR) [7]–[11]. A mismatch between the horizontal (H) and vertical (V) polarization radiation patterns, as well as a rise of

The associate editor coordinating the review of this manuscript and approving it for publication was Yasar Amin.

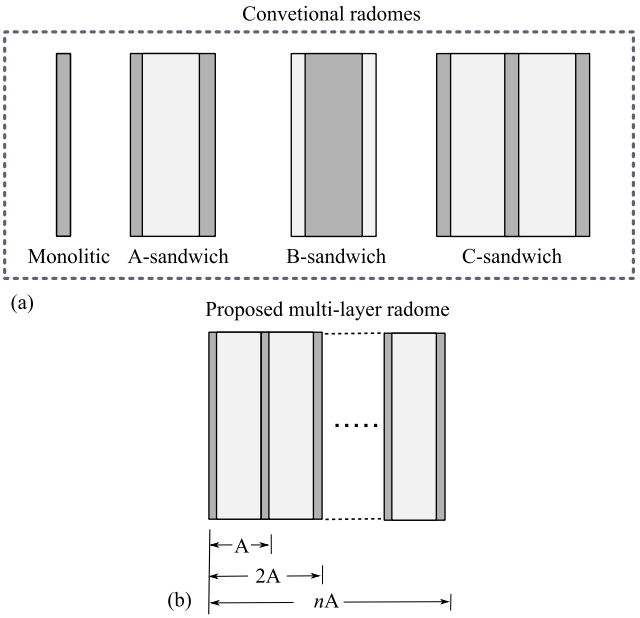

FIGURE 1. Conventional and proposed radome. In (a) Monolithic, A-sandwich, B-sandwich, C-sandwich, and in (b) Proposed multi-layer radome for ultra-wide-band applications.

the cross-polarization components, produced because of the radome, introduce a bias in the measurements of Z_{DR} and LDR [9]–[11].

The simplest radome is a single-wall structure [4], [12], which is a homogeneous half-wavelength thick dielectric material, as shown in Fig. 1a. Electromagnetic waves typically experience less reflection when impinging on the dielectric substrate in the bore-sight direction. However, reflection gets worse as the oblique incident angle increases. This condition is true especially in case of transverse-electric polarization due to the lack of Brewster's angle [13]. Furthermore, these radomes have narrow bandwidth usually not more than 6–10%. Therefore, radars are equipped with a spherical shaped radome in order to maintain the bore-sight incidence condition. In addition, these radomes are very heavy and thick at low frequencies. Another radome configuration used to minimize RF reflections is the A-sandwich radome (Fig. 1a), which consists of two thin dielectric skins separated by a core having low dielectric material [14]–[16]. The reflection can be lowered by the mutual cancellation of the reflections between the skins. This type of radome has a high strength-to-weight ratio comparing to a single wall structure. In addition, different dielectric constants and thicknesses for the skin as well as the core can be considered for optimized reflection in both E- and H-polarizations at oblique incidence angles.

In the current situation, most researchers are focusing to design one platform for multiple applications. Such as diverse types of antenna for communications, electronic warfare, weather radar, aircraft surveillance, security, and defense sectors that cover multiple frequency bands such as S-band (2 GHz - 4 GHz), C-band (4 GHz - 8 GHz), X-band (8 GHz - 12 GHz), etc., [17]. Multi-function and shared aperture capabilities reduce the number of RF systems needed during deployment and allow improved mobility and operational agility, while maintaining high spectral efficiency [18]–[23]. These multi-function radars require ultra-wide band (UWB) radomes along with a wide scanning angle in both V- and H-polarization. Besides, the radome should be thick and lightweight, A-sandwich structures can be tuned to be broadband structures, by choosing the permittivity and thickness of each layer properly. The bandwidth of this type of radomes can be further enhanced by increasing the core thickness by its integral multiples. However, this increases the overall thickness of the radome and decreases the mechanical strength due to the use of low-density material as a thick core layer [24].

Multi-layer structures may have any number of layers required to achieve desired properties such as low transmission loss over a wide frequency band or to incorporate desired environmental and structural features. In the last decade, few works have been reported for multi-layer radome specifically for UWB characteristics. A flat multi-layer radome with passbands having odd times of selected central frequency was proposed in [25]. This multi-layer radome comprises of five or more layers, in which each layer was designed as an electromagnetic matching layer at the arbitrarily selected design frequency. In another work, a graded material structure was optimized for broadband radome application by using a hybrid method [26]. In [27], another broadband graded porous wall structure with 4 layers was designed ranging from 1 GHz to 18 GHz. Another wideband flat radome using inhomogeneous planar layers was proposed in [28]. However, these radomes are expensive and have high fabrication complexity. Currently, wide band radomes have been designed using a frequency selective surfaces (FSS), which help reducing the overall thickness of the radome [29]–[31]. However, these radomes have limited bandwidth and high insertion loss due to use of conducting materials to design FSS.

In this paper, a new ultra-wide-band radome is modeled, constructed, and validated. The design methodology of the proposed multi-layer radome relies on several A-sandwich structures as shown in Figs. 1b and 2, which are not used in conventional multi-layer radome. The proposed structure allows for increasing the bandwidth while having a negligible change in the overall thickness of radome. The proposed configuration also provides greater strength and rigidity in the mechanical design and gives more degrees of freedom for the electrical design [32]. In addition, co-polarization mismatch and depolarization ratio of proposed radome have been discussed. These features are limited in previous proposed radome. Three different multi-layer radomes having three different bandwidths are designed and analyzed. The performance of the proposed radomes is analyzed using

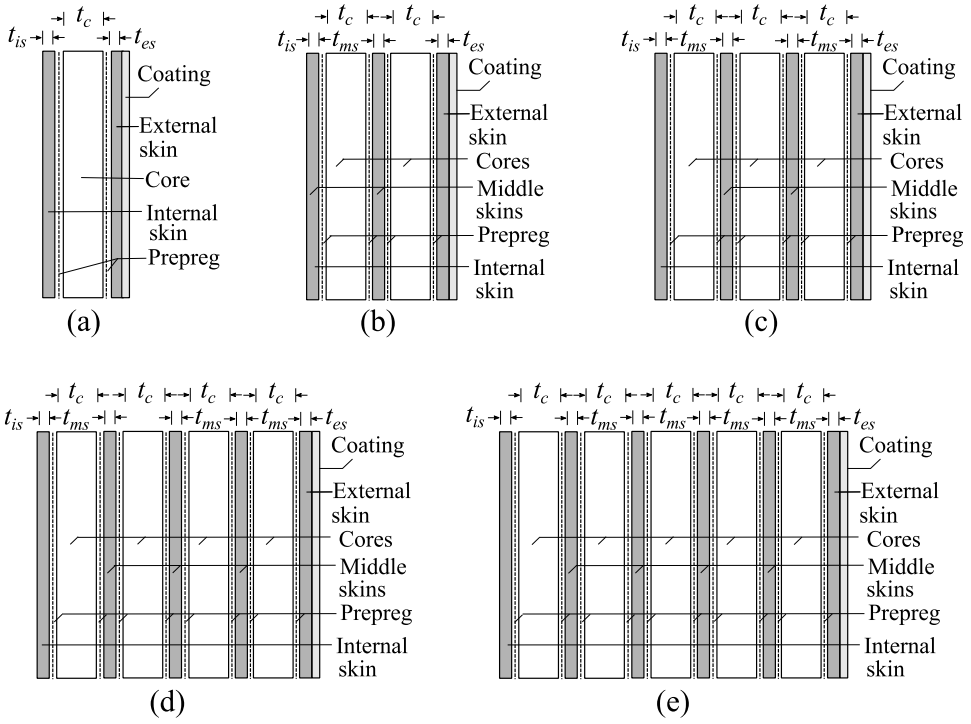

FIGURE 2. Different multi-layer radomes for different bandwidth (a) A-sandwich (b) 2A-sandwich (c) 3A-sandwich (d) 4A-sandwich (e) 5A-sandwich.

various parameters such as co-polarization mismatch and depolarization ratio. To validate the proposed design methodology, a multi-layer radome operates from 1 GHz to 14 GHz is designed, fabricated, and tested.

II. RADOME DESIGN AND REQUIREMENTS

The design procedure proposed is summarized in the flow chart illustrated in Fig.3. This procedure starts with a selection of the lowest frequency in the band required. The expression (1) can be used to compute the thickness of the core of the A-sandwich radome [24].

$$t_c = \frac{\lambda_o}{2\pi\sqrt{\varepsilon_c - \sin^2(\theta_i)}}\left[\pi - \tan^{-1}\left(\frac{Num}{Den}\right)\right] \tag{1}$$

$$Num = 2(\varepsilon_s - 1)\sqrt{\varepsilon_s\varepsilon_c}\,\sin(2\phi_s) \tag{2}$$

$$Den = (\varepsilon_s + 1)(\varepsilon_c - \varepsilon_s) + (\varepsilon_s - 1)(\varepsilon_s + \varepsilon_c)\cos(2\phi_s) \tag{3}$$

$$\phi_s = \frac{2\pi\ t_s}{\lambda_0}\sqrt{\varepsilon_s - \sin^2(\theta_i)} \tag{4}$$

where $t_{es} = t_{is} = t_s$ are the thicknesses of external and internal skin, t_c is the core thickness, ε_s is the skin permittivity, ε_c is the core permittivity, θ_i is the incident angle from the normal to the planar radome and λ_o is the free space wavelength.

Multiple A-sandwich structures can be combined to form a wideband radome. The core thickness (t_c) of each A-sandwich modifies (decreases) as the number of A-sandwiches increases. Hence, there will be a negligible change in the overall radome thickness. The core thickness (t_c) for multiple A-sandwich radome can be modified using proposed piece-wise analytical expression (5). This simplified expression is obtained by using parametric analysis based on the transmission line model [14]. The middle skin $t_{ms} = 2t_s$ has twice the thickness compared to internal and external thickness.

$$t_{c(nAsand)} = 4t_c e^{-3n} + t_c e^{-0.3n} \tag{5}$$

where n is the number of A-sandwich structures.

Middle skin layers of the proposed radome should offer sufficient mechanical strength. Whereas, the external layer of the radome should also bear environmental impacts from dust, rain, snow etc. For designing this type of high performance radomes that satisfy these conditions, two different materials either as an external or middle skin are required. These materials may have different permittivities and different thicknesses. Therefore, proposed analytical expression (6) can be used to estimate the thicknesses of different skins with respect to their permittivities.

$$t_{s2} = t_{s1}\left(\frac{\varepsilon_{s1}^2 + \varepsilon_{s1}^2\delta_{s1}^2}{\varepsilon_{s2}^2 + \varepsilon_{s2}^2\delta_{s2}^2}\right)^{1/4} \tag{6}$$

where δ is the tangent loss.

A. BANDWIDTH

The bandwidth of the radome is highly dependent upon the number of A-sandwiches. As the number of A-sandwiches increases, the bandwidth increases with a trade-off of slight increment in radome thickness. The approximate percentage

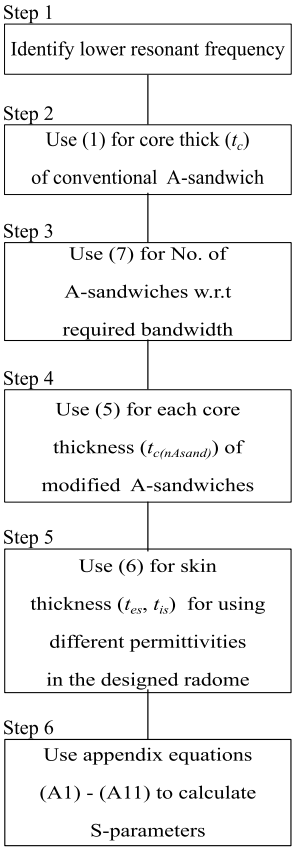

FIGURE 3. Flow-chart of proposed radome design.

bandwidth of the radome can be calculated by using the proposed analytical expression (7). This expression is also derived using parametric analysis based on the transmission line model proposed in [14].

$$BW(\%) = 125e^{\frac{n}{20}} - 159e^{-\frac{5}{4}n} \tag{7}$$

B. CO-POLARIZATION MISMATCH

There are two main polarization components (horizontal and vertical) of plane wave incident onto the radome's wall. The transmission difference between these components is the main factor in many applications. For example in dual polarized weather radar systems, the main goal of active phased array antenna is to maintain a differential reflectivity (Z_{DR}) better than 0.1 dB, which is the transmission difference between H- and V-polarization components in logarithmic form [33], [34]. Transmission difference between H- and V-polarization of a radome creates a mismatch (CM_{dB}) in co-polarization radiation patterns of antenna systems. This causes errors in the measurements of radar systems. The CM_{dB} is given by

$$CM_{dB} = T_V - T_H \tag{8}$$

where T_V and T_H are the transmissions of the V- and H-polarization components, respectively.

TABLE 1. Material constitutive parameters.

Layers	Permittivity (ε_r)	Tangent loss (δ)
External / internal skin	2.2	0.0009
Middle skin	3.48	0.004
Core	1.09	0.0038

TABLE 2. Proposed radome types and thicknesses.

Types	Thickness (in mils)				
	Core (t_c)	Ext. skin (t_{es})	Mid. skin (t_{ms})	Int. skin (t_{is})	Total (t)
A	1030	60	-	60	1150
2A	500	60	30	60	1150
3A	375	50	30	50	1285
4A	300	40	20	40	1340
5A	250	30	20	30	1370

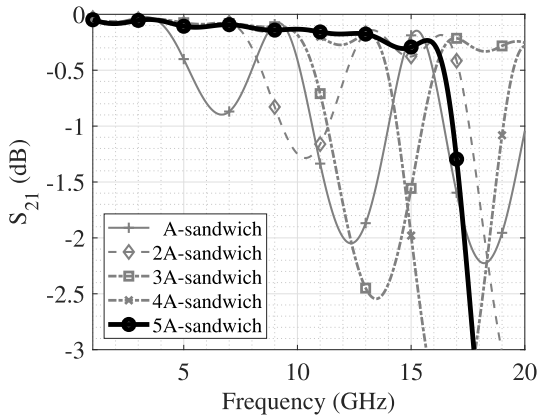

FIGURE 4. S_{21} vs. frequency of different multi-layer radomes.

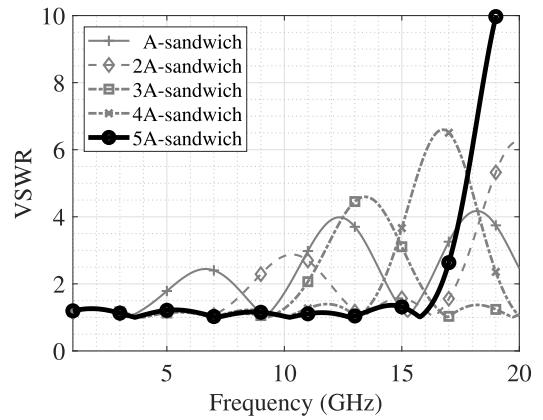

FIGURE 5. VSWR vs. frequency of different multi-layer radomes.

C. DEPOLARIZATION RATIO

The transmission difference of H- and V-polarization components can also affect the depolarization ratio (DPR). When this ratio is high, it deteriorates the cross-polarization performance of the radar or communication system. e.g for an antenna with −40 dB cross-polarization enclosed by a radome having a depolarization ratio of −10 dB, the total

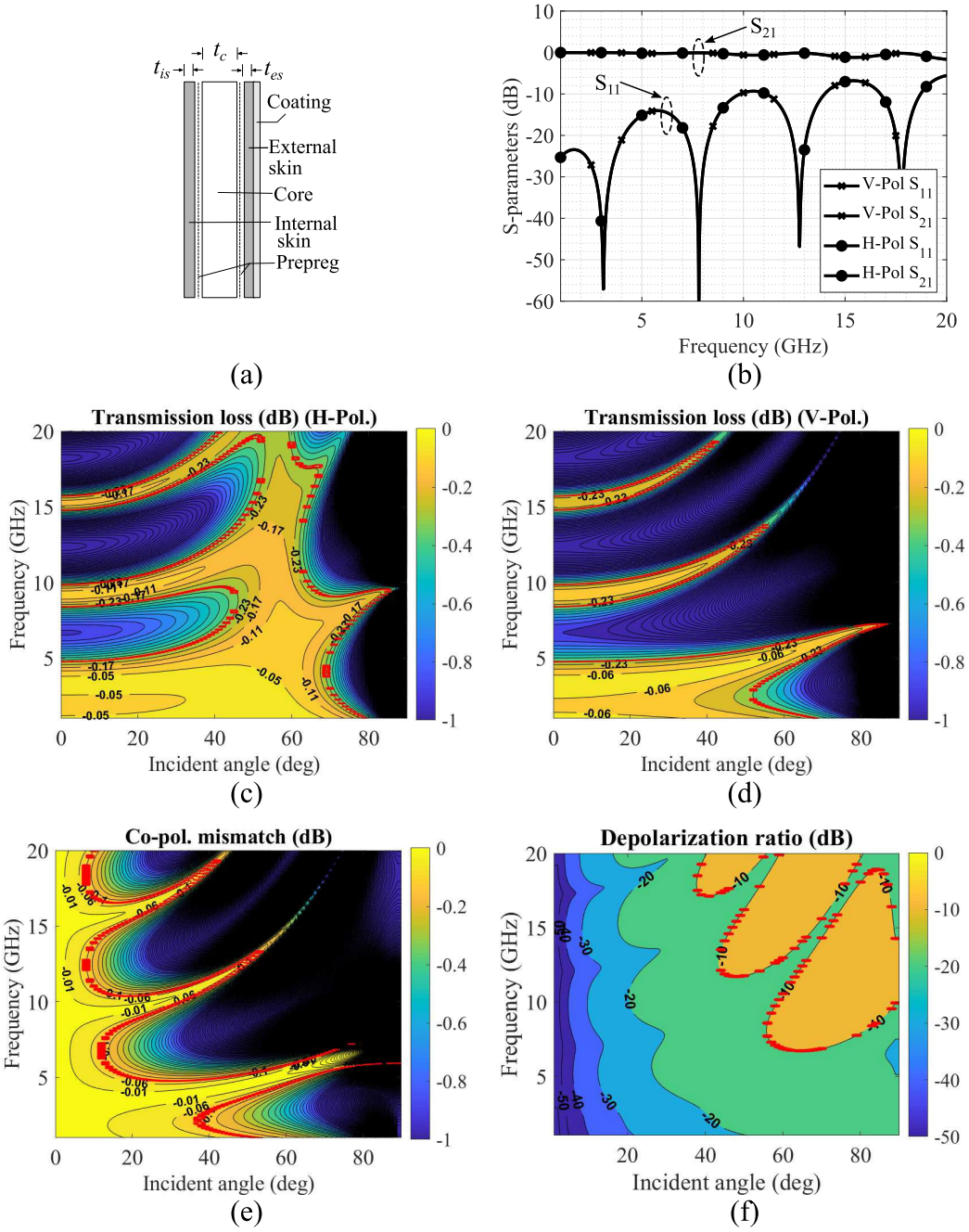

FIGURE 6. Multi-layer: A-sandwich radome (a) Schematic (b) *S*-parameters (c) H-pol transmission loss (d) V-pol transmission loss (e) Co-polarization mismatch (f) Depolarization ratio.

cross-polarization would be −30 dB. This adverse effect is critical for a polarimetric radar system that requires high isolation (<−40 dB) between polarization channels [7], [8], [35]. The intensity of the depolarization ratio depends on the amplitude and phase of the complex transmission coefficients of both polarizations. And these coefficients depend upon the incident angle and the tilt of the plane of polarization. All these parameters must be determined and taken into account at the appropriate stage. For purely V- or H-polarization, the cross-polarization vanishes, as in each case, one of the resolved components is zero. This depolarization ratio of any radome type can be calculated using (9) [14].

$$DPR = \sqrt{\frac{1 - 2kcos(\phi_V - \phi_H) + k^2}{cot^2\theta_i + 2kcos(\phi_V - \phi_H) + k^2 tan^2\theta_i}} \tag{9}$$

where $k = |T_V| \,/\, |T_H|$ and $(\phi_V - \phi_H)$ is the phase difference of respective polarizations.

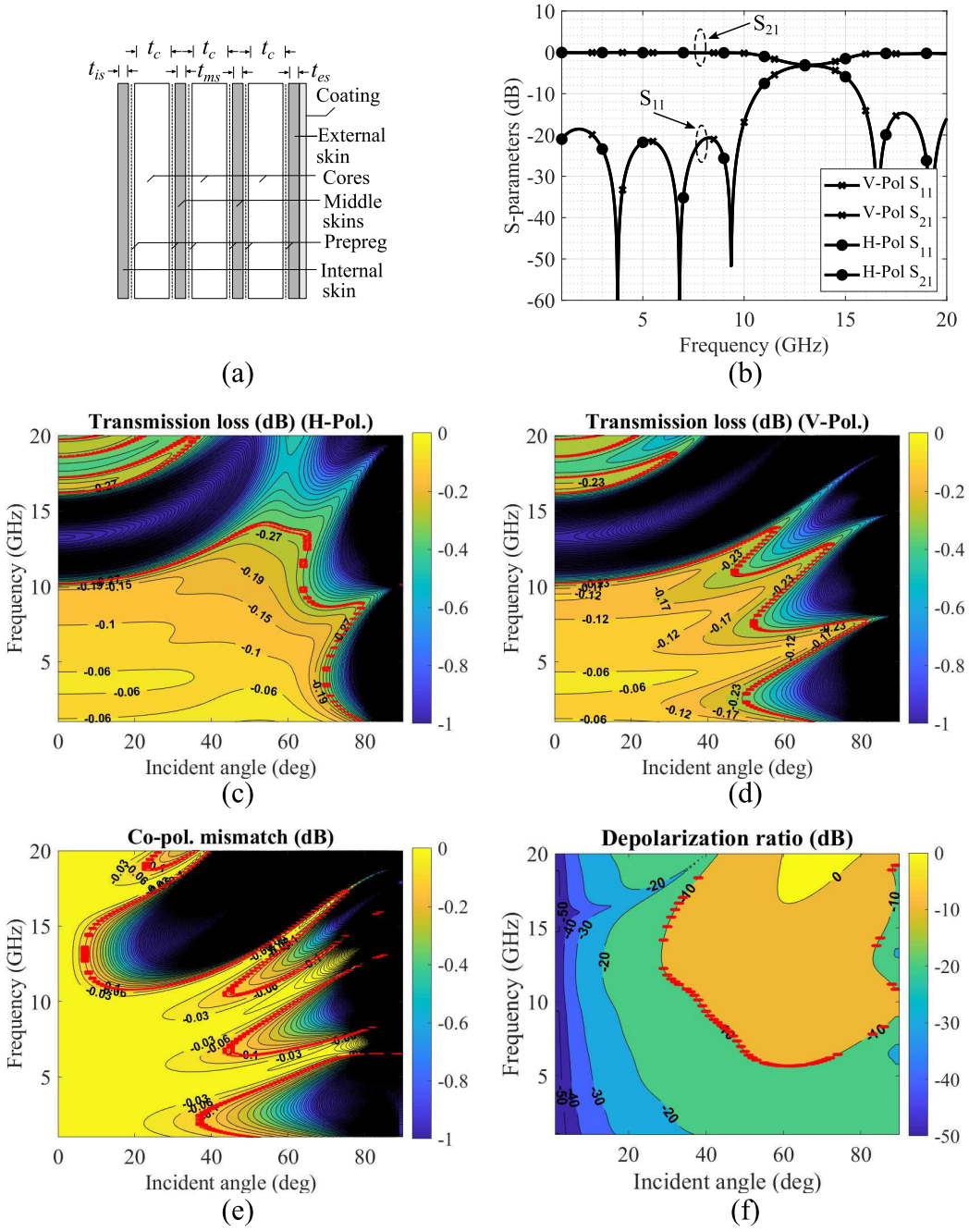

FIGURE 7. Multi-layer: 3A-sandwich radome (a) Schematic (b) *S*-parameters (c) H-pol transmission loss (d) V-pol transmission loss (e) Co-polarization mismatch (f) Depolarization ratio.

III. PROPOSED MULTI-LAYER RADOMES

Based on the design guidelines, shown in Fig. 3, equations (1) - (7) are used to obtain the dimensions (thickness) of each layer of these multi-layer radomes for different bandwidths. Table 1 presents the constitutive electrical parameters of materials of different radome types, and Table 2 presents the calculated thickness of each layer. The transmission line model in the appendix section (A1) - (A11) [14] is then used to obtain the insertion loss S_{21} and voltage standing wave ratio (VSWR) of these radomes. It can be seen in Figs. 4 and 5, the bandwidth of each radome increases as the number of A-sandwiches increases. Considering a threshold of $S_{21} \geq$ -0.4 dB and VSWR $\leq$ 2, A-sandwich radome has 86%, 2A-sandwich has 125%, 3A-sandwich has 140% and 4A-sandwich has 151% and 5A-sandwich has 158% bandwidths.

Three proposed multi-layer radomes (A-sandwich, 3A-sandwich, and 5A-sandwich) are further analyzed

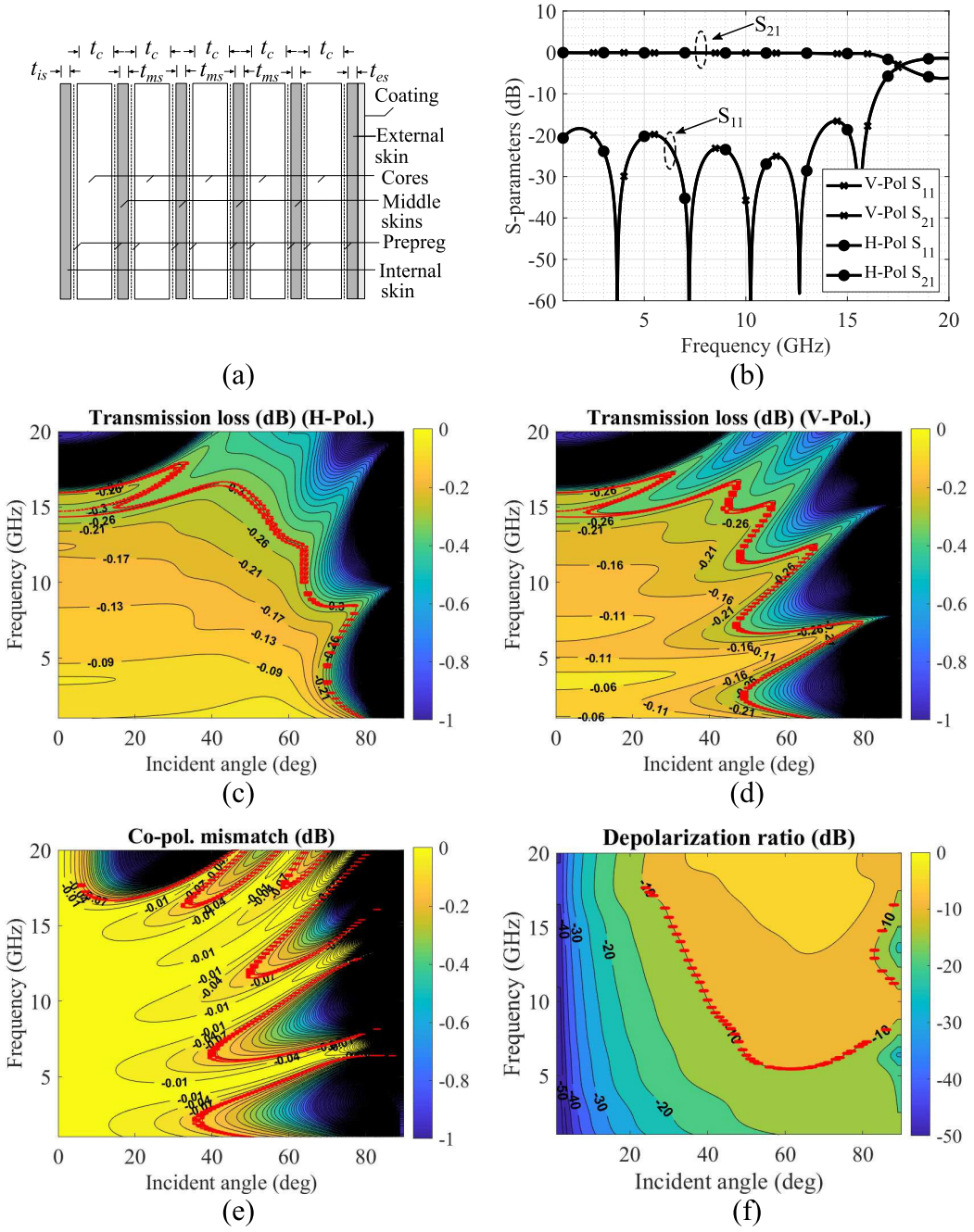

FIGURE 8. Multi-layer: 5A-sandwich radome (a) Schematic (b) *S*-parameters (c) H-pol transmission loss (d) V-pol transmission loss (e) Co-polarization mismatch (f) Depolarization ratio.

using formulation presented in [14]. The first radome is A-sandwich radome, as shown in Fig. 6a. The total thickness of this radome is 1.15in, as shown in Table 3. This radome operates from 1 GHz to 4 GHz (Fig. 6b) and presents an insertion loss of 0.053 dB for H- and V-polarizations. Fig. 6c,d shows a 2-D graph of insertion loss for both polarizations at oblique incident angles. The red line is an insertion loss threshold equals to 0.3 dB, which shows that radome works up to 55°. The 0.1 dB mismatch as a threshold can be observed in both polarizations for an oblique incident angle up to 39°, as shown in Fig. 6e. The depolarization ratio should be better than -10 dB. This radome shows good performance in its respected bandwidth at an incident angle up to 90°, as shown in Fig. 6f.

The second radome is the combination of three modified A-sandwich structures, as shown in Fig. 7a. It can be seen in Table 3, the overall thickness of the proposed radome is slightly increased by 0.13in. This radome operates from 1 GHz to 9 GHz (Fig. 7b) and presents an insertion loss of 0.11 dB in both H- and V-polarizations. Fig. 7c, d shows

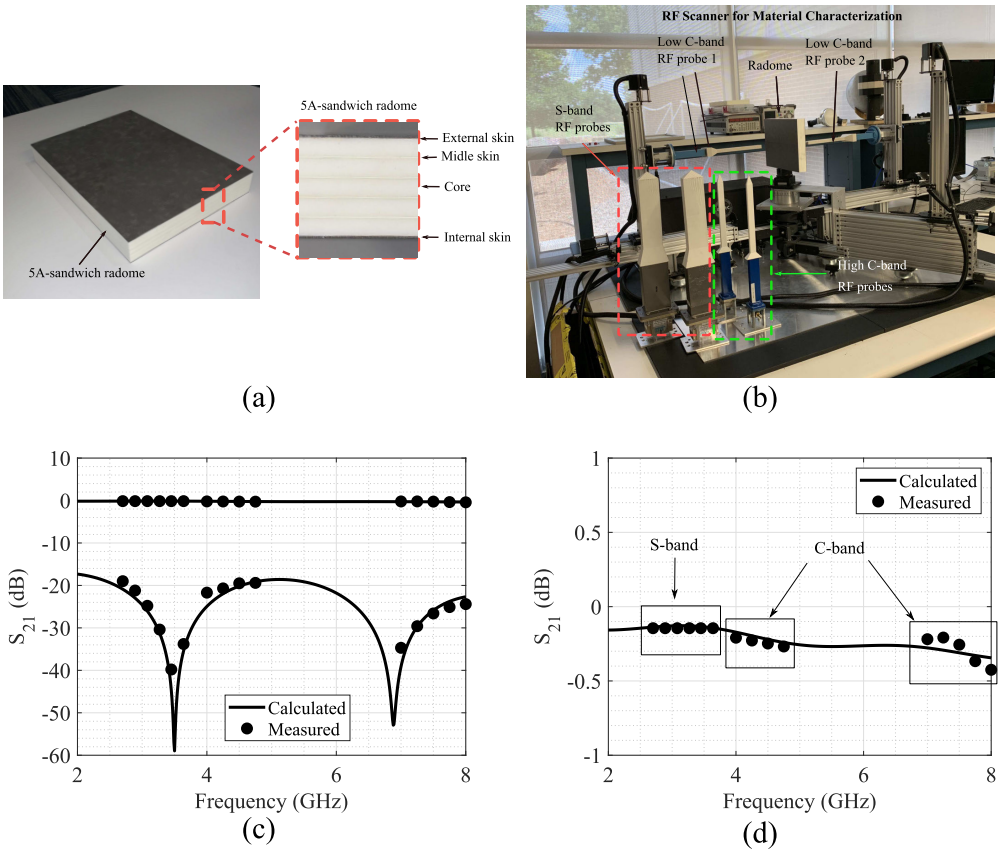

FIGURE 9. Validation of 5A-sandwich (a) Prototype (b) Measurement setup for testing in S-band and C-band (c) Simulated and measured *S*-parameters (d) Simulated and measured S_{21}.

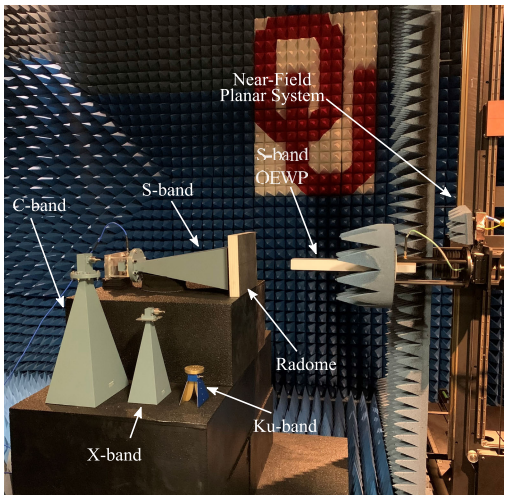

FIGURE 10. Measurement setup for 5A-sandwich radome for testing in S-band, C-band, X-band and Ku-band using the near-field planar range system.

2-D insertion loss for both polarizations for oblique incident angles. Similarly to the first radome, the red line represents the threshold equals to 0.3 dB, which shows that this radome also works up to 54°. The 0.1 dB co-polarization mismatch (Fig. 7e) as a threshold can be observed in both polarizations for an oblique incident angle up to 39°. As shown in Fig. 7f,

TABLE 3. Performance of proposed A-, 3A- and 5A-sandwich radome types.

Types	BW (GHz) (VSWR≤2)	t (in)	Maximum incident angle		
			IL ≤0.3 dB	CM ≤0.1 dB	DPR ≤-10 dB
A	1-4	1.15	55°	39°	90°
3A	1-4	1.28	50°	39°	90°
	5-9		54°	48°	43°
5A	1-4	1.37	50°	37°	90°
	5-9		50°	41°	46°
	9-14		55°	54°	39°

BW : Bandwidth, t : thickness, DPR: Depolarization ratio.
IL : Insertion loss, CM : Co-polarization mismatch.

the depolarization ratio is reduced to 43° with respect to -10 dB threshold as the bandwidth of this radome is wider than the previous one.

The third radome is the combination of five modified A-sandwich structures, as shown in Fig. 8a. It can be seen in Table 3, the overall thickness of the proposed radome is 1.37in, which is slightly increased by 0.22in and 0.09in compare to A-sandwich and 3A-sandwich radome, respectively. The proposed radome can operate from 1 GHz to 14 GHz (Fig. 8b) and presents an insertion loss of 0.2 dB for both polarizations. Fig. 8c, d shows 2-D insertion loss for both polarizations at oblique incident angles. Similarly to previous radomes, the red line represents the 0.3 dB

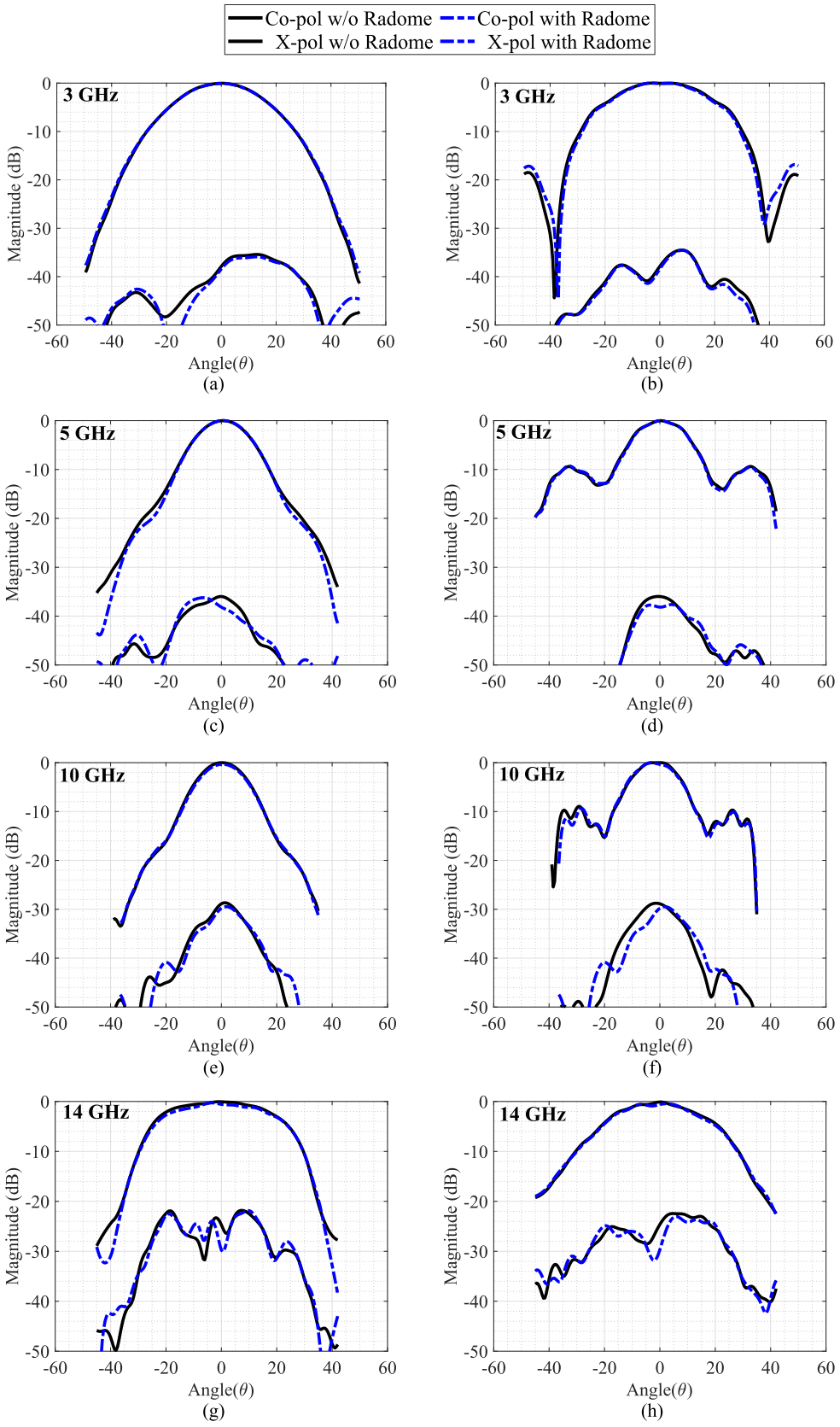

FIGURE 11. Measured co- and cross-polarization radiation patterns of horn antennas with and without proposed radomes (a) E-plane @ 3 GHz (b) H-plane @ 3 GHz (a) E-plane @ 5 GHz (b) H-plane @ 5 GHz (a) E-plane @ 10 GHz (b) H-plane @ 10 GHz (a) E-plane @ 14 GHz (b) H-plane @ 14 GHz.

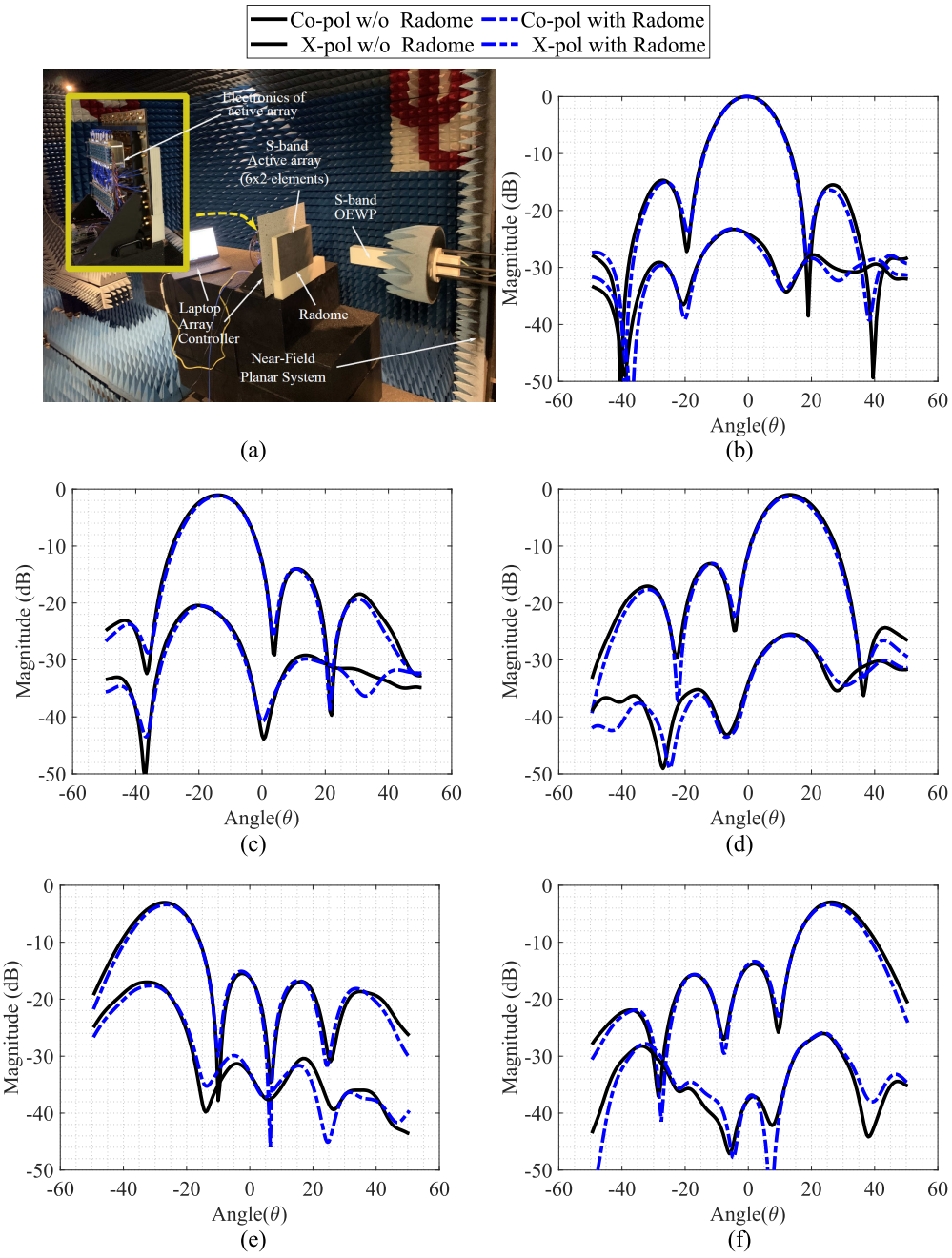

FIGURE 12. (a) Measurement setup. Measured co- and cross-polarization radiation patterns of microstrip phased array at 3 GHz with and without proposed radomes at oblique angles (b) 0° (c) −15° (d) +15° (e) −30° (f) +30°.

threshold, which shows that radome works up to 50°. The 0.1 dB co-polarization mismatch (Fig. 8e) can be observed in both polarizations for an oblique incident angle up to 37°. As shown in Fig. 8f, again the depolarization ratio has slightly reduced up to 39° incident angle for the entire bandwidth.

IV. VALIDATION OF THE PROPOSED RADOME

To validate the proposed design, the 5A-sandwich radome is constructed using RF materials available in our laboratory that have a similar performance of materials used by companies that develop operational radomes. Fig. 9 shows a picture of the 5A-sandwich radome and close up picture of the radome stack-up. Polytetrafluoroethylene (PTFE) material with $\varepsilon_r = 2.2$ and $\delta = 0.0009$ is used as an external/internal skin layers due to its hydrophobic properties. The advantages of using Teflon based material to obtain wetless radome surface are discussed in detail in [6], [35]. PTFE provides very low δ (0.0009 at 10 GHz) and offers great chemical resistant properties, small water absorption, and high-temperature resistance. Rogers 4350B with ε_r equals to 3.48 and δ of 0.004 is used as middle skin layers. For core material, Rohacell 71HF with ε_r of 1.09 and δ of 0.0038 is

TABLE 4. Performance of proposed 5A-sandwich radome as a function of frequency.

f	Calculated* losses (dB)	Measured** losses (dB)	Absolute error (dB)
3 GHz	0.1293	0.1140	0.0153
5 GHz	0.2200	0.2562	0.0362
10 Ghz	0.3010	0.3121	0.0210
14 Ghz	0.3764	0.4183	0.0419

(*) Losses based on model [14].
(**) Losses based on measured radiation patterns.

TABLE 5. Performance of proposed 5A-sandwich radome at 3 GHz as a function of incident angle.

θ	Calculated* losses (dB)	Measured** losses (dB)	Absolute error (dB)
-30°	0.2328	0.3270	0.0942
-15°	0.1861	0.2500	0.0639
0°	0.1293	0.1760	0.0467
15°	0.1861	0.2210	0.0349
30°	0.2328	0.3110	0.0782

(*) Losses based on model [14].
(**) Losses based on measured radiation patterns.

used. These materials are joined together by using epoxy resin as a bond-ply/prepreg. The measured ε_r and δ of epoxy are 2.83 and 0.09, respectively. All these commercially available materials are used to validate the concept of achieving a multi-layer radome with ultra-wide bandwidth characteristics. Fig. 9b shows the measurement setup along with dielectric rod antennas that work in S- and C-bands. These rod antennas have a narrow bandwidth, that restricts the complete measurement of the proposed radome. The S-band antenna is used to measure the frequency range from 2.7 GHz to 3.6 GHz and the other two C-band antennas are used to measure the frequency range from 4 GHz to 4.8 GHz and 7.1 GHz to 8 GHz, respectively. The simulated and measured S-parameters are in a good agreement as shown in Fig 9c, d.

For the evaluation of the proposed structure, radiation patterns of horn antennas at 3 GHz, 5 GHz, 10 GHz, and 14 GHz are measured with and without proposed radome in the near-field anechoic chamber at Radar Innovation Laboratory at The University of Oklahoma, as shown in Fig. 10. The co- and cross-polarization radiation patterns of these horn antennas with and without radomes are in good correspondence, as shown in Fig. 11. It can be seen in Table 4, the losses with and without the proposed radome, is recorded as 0.114 dB at 3 GHz, 0.2562 dB at 5 GHz, 0.3121 dB at 10 GHz and 0.4183 dB at 14 GHz, in the bore-sight direction.The absolute errors between calculated and measured values at all frequencies are below 0.05 dB.

The proposed radome is also evaluated by measuring the radiation patterns of an electronically scanned active phased array antenna at 3 GHz for an oblique angles from $-30°$ to $+30°$ in the near field chamber as shown in Fig. 12. Table 5 presents the measured losses of an active phased array with and without radome as 0.176 dB, 0.250 dB, 0.221 dB, 0.327 dB and 0.311 dB at 0°, $-15°$, $+15°$, $-30°$, $+30°$, respectively. The absolute errors between the calculated and measured values at all scanning angles below 0.1 dB.

TABLE 6. Comparison of proposed radome performance with previous work.

	Type	BW (GHz)	t (mil)	IL (dB)	FC	CM	DPR
This Work	ML	1-14	1370	0.4183	Low	Yes	Yes
Ref [25]	ML	2-25	788	0.9	High	No	No
Ref [26]	ML	1-18	788	1.74	High	No	No
Ref [27]	ML	1-18	237	3.09	High	No	No
Ref [28]	ML	1-8	3937	0.9	High	No	No
Ref [29]	FSS	3.4-12.1	157	1	Low	No	No
Ref [30]	FSS	8-14	190	0.91	Low	No	No
Ref [31]	FSS	7.5-15	436	0.969	Low	No	No

BW: Bandwidth, t: thickness, FC : Fabrication complexity,
IL: Insertion loss, ML: Multi-layer, FSS: Frequency selective surfaces.
DPR: Depolarization ratio, CM: Co-polarization mismatch.

The proposed radome is compared with previous work. As summarized in Table 6, the proposed radome discussed about co-polarization mismatch and depolarization (cross-polarization) ratio, which are highly required parameters for dual polarized applications. Moreover, all previous structures have high insertion loss compared to proposed radome, which is less than 0.5 dB in the broadside. FSS based wideband radomes, presented in [25]–[27], are thinner than proposed radomes due to small number of layers. However, these radomes have limited bandwidth. The proposed radome covers the frequency range from 1 GHz to 14 GHz, which is narrower than the multilayer structures presented in [29]–[31]. However, the materials used in these radomes have different permittivities and are required to develop separately. Therefore, the fabrication complexity in all these radomes is also high. The presented technique allows utilizing the commercially available materials to design the proposed radome.

V. CONCLUSION

In this paper, a new technique to design an ultra-wide-band, high performance, multi-layer radome for dual-polarized radar and communication systems is presented. The proposed radome provides excellent RF performance, thermal isolation, and mechanical strength. Co-polarization mismatch less than 0.1 dB and depolarization ratio better than 10 dB for oblique incident angles up to 40° is recorded, which is ideal for dual-polarized weather radars. To validate the proposed radome design technique, a multi-layer radome with ultrawideband characteristics that operates from 1 GHz to 14 GHz is designed, fabricated, and tested. Calculated and measured results are in excellent agreement. The RF performance of the proposed radome is also evaluated by measuring the radiation patterns of horn antennas at four different frequencies i.e. 3 GHz, 5 GHz, 10 GHz and 14 GHz. The measured losses with and without proposed radome are recorded as 0.114 dB, 0.2562 dB, 0.3121 dB and 0.4183 dB with absolute errors below 0.05 dB compared to calculated values. Moreover, the radiation patterns of an electronically scanned active phased array antenna for 3 GHz frequency at

different scanning angles, with and without proposed radome are also measured and evaluated. The losses are 0.176 dB, 0.250 dB, 0.221 dB, 0.327 dB and 0.311 dB at 0°, −15°, +15°, −30°, +30°, respectively. The absolute errors between the calculated and measured values at all scanning angles are below 0.1 dB. The proposed radome can be used in different applications ranges from 1 GHz to 14 GHz, such as surveillance systems, earth exploration satellite, aeronautical radionavigation, and especially in dual-polarized weather radars that require a high parametric performance. The proposed method can be implemented for higher frequencies.

APPENDIX

The equivalent transmission line model has also been implemented to extract the frequency response of different types of radomes [14]. This model can use lossy dielectrics, therefore, they are fully characterized by ε and δ, whereas the permeability $\mu = 1$ is considered. Equations (A1)-(A11) are used to calculate the overall reflection and transmission coefficients of proposed radome for perpendicular and parallel polarizations.

$$\Gamma_V = \frac{B_0}{A_0}, \quad T_V = \frac{1}{A_0} \tag{A1}$$

$$\Gamma_H = \frac{D_0}{C_0}, \quad T_H = \frac{1}{C_0} \tag{A2}$$

The A_0, B_0, C_0 and D_0 are found using the recursive formulas

$$A_n = \frac{e^{+\psi_n}}{2}[A_{n+1}(1+Y_{n+1}) + B_{n+1}(1-Y_{n+1})] \tag{A3}$$

$$B_n = \frac{e^{-\psi_n}}{2}[A_{n+1}(1-Y_{n+1}) + B_{n+1}(1+Y_{n+1})] \tag{A4}$$

$$C_n = \frac{e^{+\psi_n}}{2}[C_{n+1}(1+Z_{n+1}) + D_{n+1}(1-Z_{n+1})] \tag{A5}$$

$$D_n = \frac{e^{-\psi_n}}{2}[C_{n+1}(1-Z_{n+1}) + D_{n+1}(1+Z_{n+1})] \tag{A6}$$

where

$$A_{N+1} = C_{N+1} = 1, \quad B_{N+1} = D_{N+1} = 0 \tag{A7}$$

$$Y_{n+1} = \frac{cos\theta_{n+1}}{cos\theta_n}\sqrt{\frac{\varepsilon_{n+1}(1-j\delta_{n+1})\mu_n}{\varepsilon_n(1-j\delta_n)\mu_{n+1}}} \tag{A8}$$

$$Z_{n+1} = \frac{cos\theta_{n+1}}{cos\theta_n}\sqrt{\frac{\varepsilon_n(1-j\delta_n)\mu_{n+1}}{\varepsilon_{n+1}(1-j\delta_{n+1})\mu_n}} \tag{A9}$$

$$\psi_n = t_n\gamma_n cos\theta_n \tag{A10}$$

$$\gamma_n = \sqrt{j\omega\mu_n(\sigma_n + j\omega\varepsilon_n)} = j\omega\sqrt{\mu_n\varepsilon_n(1-j\delta_n)} \tag{A11}$$

where $n = 0, 1, 2, 3, \ldots, N$, where N is the number of layers, t_n is the thickness of each layer, δ is the tagent-loss and θ_n is the complex angle of refraction in the n^{th} layer.

ACKNOWLEDGMENT

The authors would like to thank the Advanced Radar Research Center (ARRC) at The University of Oklahoma for providing the facilities needed to perform this research. They would also like to thank all members of the Phased Array Antenna Research and Development group (PAARD) for the discussions and positive feed-backs.

REFERENCES

[1] J. D. Walton, *Radome Engineering Handbook: Design and Principles*. New York, NY, USA: Marcel Dekker, 1970.
[2] J. A. Vitale, *Microwave Scanning Antennas*, vol. 1. Westport, CT, USA: Peninsula Publishing, 1985, ch. 5.
[3] C. E. Hendrix, J. E. McNally, and R. A. Monzingo, "Depolarization and attenuation effects of radomes at 20 GHz," *IEEE Trans. Antennas Propag.*, vol. AP-37, no. 3, pp. 320–328, Mar. 1989.
[4] D. J. Kozakoff, *Analysis Radome-Enclosed Antennas*. Norwood, MA, USA: Artech House, 2010.
[5] A. Mancini, R. M. Lebron, and J. L. Salazar, "The impact of a wet *S*-band radome on dual-polarized phased-array radar system performance," *IEEE Trans. Antennas Propag.*, vol. 67, no. 1, pp. 207–220, Jan. 2019.
[6] J. Díaz, J. L. Salazar, A. Mancini, and J. G. Colom, "Radome Design and Experimental Characterization of Scattering and Propagation Properties for Atmospheric Radar Applications," in *Proc. Amer. Meteorol. Soc.*, 2014, pp. 819–823.
[7] D. S. Zrnić and R. J. Doviak, "System requirements for phased array weather radar," NOAA/NSSL, Washington, DC, USA, NOAA/NSSL Rep., 2005. [Online]. Available: https://www.nssl.noaa.gov/publications/mpar_reports/LMCO_Consult2.pdf
[8] Y. Wang and V. Chandrasekar, "Polarization isolation requirements for linear dual-polarization weather radar in simultaneous transmission mode of operation," *IEEE Trans. Geosci. Remote Sens.*, vol. 44, no. 8, pp. 2019–2028, Aug. 2006.
[9] S. J. Frasier, F. Kabeche, J. F. i Ventura, H. Al-Sakka, P. Tabary, J. Beck, and O. Bousquet, "In-place estimation of wet radome attenuation at x band," *J. Atmos. Ocean. Technol.*, vol. 30, no. 5, pp. 917–928, May 2013.
[10] E. Gorgucci, R. Bechini, L. Baldini, R. Cremonini, and V. Chandrasekar, "The influence of antenna radome on weather radar calibration and its real-time assessment," *J. Atmos. Ocean. Technol.*, vol. 30, no. 4, pp. 676–689, Apr. 2013.
[11] M. Schneebeli, J. Sakuragi, T. Biscaro, C. F. Angelis, I. C. Da Costa, C. Morales, L. Baldini, and L. A. T. Machado, "Polarimetric X-band weather radar measurements in the tropics: Radome and rain attenuation correction," *Atmos. Meas. Techn.*, vol. 5, no. 9, pp. 2183–2199, Sep. 2012.
[12] H. L. Hirsch, *Practical Simulation of Radar Antennas and Radomes*. Norwood, MA, USA: Artech House, 1987.
[13] D. Burks, *Antenna Engineering Handbook, Chapter 53 Radomes*. New York, NY, USA: McGraw-Hill, 2007.
[14] Z. Qamar, N. Aboserwal, and J. L. Salazar-Cerreno, "An accurate method for designing, characterizing, and testing a multi-layer radome for mm-wave applications," *IEEE Access*, vol. 8, pp. 23041–23053, 2020.
[15] X. Tang, W. Zhang, and J. Zhu, "Multidisciplinary optimization of airborne radome using genetic algorithm," in *Proc. Int. Conf. Artif. Intell. Comput. Intell.* Berlin, Germany: Springer, 2009, pp. 150–158.
[16] F. Mazlumi, "Analysis and design of flat asymmetrical a-sandwich radomes," *J. Telecommun., Electron. Comput. Eng. (JTEC)*, vol. 10, no. 3, pp. 9–13, 2018.
[17] J. L. Salazar-Cerreno, Z. Qamar, S. Saeedi, B. Weng, and H. S. Sigmarsson, "Frequency agile microstrip patch antenna using an anisotropic artificial dielectric layer (AADL): Modeling and design," *IEEE Access*, vol. 8, pp. 6398–6406, 2020.
[18] G. C. Tavik, C. L. Hilterbrick, J. B. Evins, J. J. Alter, J. G. Crnkovich, J. W. de Graaf, W. Habicht, G. P. Hrin, S. A. Lessin, D. C. Wu, and S. M. Hagewood, "The advanced multifunction RF concept," *IEEE Trans. Microw. Theory Techn.*, vol. 53, no. 3, pp. 1009–1020, Mar. 2005.
[19] R. W. Kindt and M. N. Vouvakis, "Analysis of a wavelength-scaled array (WSA) architecture," *IEEE Trans. Antennas Propag.*, vol. 58, no. 9, pp. 2866–2874, Sep. 2010.
[20] R. Mital, B. L. Rao, D. P. Patel, and G. C. Tavik, "Wideband multifunction array architectures using wavelength-scaled radiating elements," in *Proc. IEEE Int. Symp. Phased Array Syst. Technol.*, Oct. 2013, pp. 588–592.
[21] R. Kindt, R. Mital, J. Logan, and M. Vouvakis, "Dual-polarized sliced notch array—Ultra-wideband flares with exceptional polarization control," in *Proc. IEEE Int. Symp. Phased Array Syst. Technol. (PAST)*, Oct. 2016, pp. 1–5.
[22] R. Kindt, R. Mital, J. Logan, M. Lee, and M. Vouvakis, "A 6:1 bandwidth PUMA array at 7 mm scale," in *Proc. IEEE Int. Symp. Phased Array Syst. Technol. (PAST)*, Oct. 2016, pp. 1–4.

[23] J. T. Logan, R. W. Kindt, M. Y. Lee, and M. N. Vouvakis, "Opportunities and Advances in Ultra-wide band Electronically Scanned Arrays," in *Proc. IEEE Int. Symp. Antennas Propag. (APSURSI)*, Jun. 2016, pp. 431–432.
[24] W. M. Cady, M. B. Karelitz, and L. A. Turner, *Radar Scanners and Radomes*, vol. 26. New York, NY, USA: McGraw-Hill, 1948.
[25] L. C. Zhou, Y. M. Pei, R. B. Zhang, and D. N. Fang, "A multilayer radome wall structure with passbands having odd times of selected central frequencies," *J. Electromagn. Waves Appl.*, vol. 26, no. 16, pp. 2154–2164, 2012.
[26] Y. Zhang, Z. Zhao, Z.-P. Nie, and Q. H. Liu, "Optimization of graded materials for broadband radome wall with DRR control using a hybrid method," *Prog. Electromagn. Res. M*, vol. 43, pp. 193–201, 2015.
[27] F. Chen, Q. Shen, and L. Zhang, "Electromagnetic optimal design and preparation of broadband ceramic radome material with graded porous structure," *Prog. Electromagn. Res.*, vol. 105, pp. 445–461, 2010.
[28] M. Khalaj-Amirhosseini, "Wideband flat radomes using inhomogeneous planar layers," *Int. J. Antennas Propag.*, vol. 2008, pp. 1–6, Apr. 2008.
[29] B. Hua, X. Liu, X. He, and Y. Yang, "Wide-angle frequency selective surface with ultra-wideband eesponse for aircraft stealth designs," *Prog. Electromagn. Res. C*, vol. 77, pp. 167–173, 2017.
[30] Y. Zhao, J. Fu, Z. Liang, Z. Zhang, Z. Wang, K. Zhang, X. Ding, and G. Yang, "A novel ultra-wideband switch-type active frequency selective surface for radome applications," in *Proc. 13th Eur. Conf. Antennas Propag. (EuCAP)*, Mar. 2019, pp. 1–4.
[31] K. K. Varikuntla and R. Singaravelu, "Design of a hybrid a-sandwich radome uing a strongly coupled frequency selective surface element," *Int. J. Microw. Wireless Technol.*, vol. 12, pp. 1–11, Feb. 2020.
[32] B. Rulf, "Problems of radome design for modern airborne radar," *MiJo*, vol. 28, pp. 145–148, Jan. 1985.
[33] A. Mancini, J. L. Salazar, R. M. Lebrón, and B. L. Cheong, "A novel instrument for real-time measurement of attenuation of weather radar radome including its outer surface—Part I: The concept," *J. Atmos. Ocean. Technol.*, vol. 35, no. 5, pp. 953–973, May 2018.
[34] A. Mancini, J. L. Salazar, R. M. Lebrón, and B. L. Cheong, "A novel instrument for real-time measurement of attenuation of weather radar radome including its outer surface—Part II: Applications," *J. Atmos. Ocean. Technol.*, vol. 35, no. 5, pp. 975–991, May 2018.
[35] J. L. Salazar-Cerreño, V. Chandrasekar, J. M. Trabal, P. Siquera, R. Medina, E. Knapp, and D. J. McLaughlin, "A drop size distribution (DSD)-based model for evaluating the performance of wet radomes for dual-polarized radars," *J. Atmos. Ocean. Technol.*, vol. 31, no. 11, pp. 2409–2430, Nov. 2014.

ZEESHAN QAMAR (Member, IEEE) received the B.Sc. and M.Sc. degrees in electrical engineering from COMSATS University, Islamabad, Pakistan, in 2010 and 2013, respectively, and the Ph.D. degree in electronic engineering from the City University of Hong Kong, Hong Kong, in 2017. From July 2010 to August 2013, he was a Research Associate with the Department of Electrical and Computer Engineering, COMSATS University. From November 2017 to April 2018, he was a Postdoctoral Research Associate with the Department of Materials Science and Engineering, City University of Hong Kong. He is currently a Postdoctoral Research Fellow with the Phased Array Antenna Research and Development Group (PAARD) and the Advanced Radar Research Center (ARRC), The University of Oklahoma, Norman, OK, USA. His current research interests include microwave/millimeter-wave circuits, material characterization, meta-materials, artificial dielectric layer, antennas and phased arrays, and phased array antennas. He is a member of the IEEE Antennas and Propagation Society (AP-S), and a Reviewer of various conferences and journals.

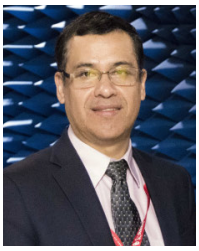

JORGE L. SALAZAR-CERRENO (Senior Member, IEEE) received the B.S. degree in ECE from the University Antenor Orrego, Trujillo, Peru, the M.S. degree in ECE from the University of Puerto Rico, Mayagüez (UPRM), and the Ph.D. degree in ECE from the University of Massachusetts, Amherst, in 2011. His Ph.D. research focused on development of low-cost dual-polarized active phased array antennas (APAA). After graduation, he was awarded a prestigious National Center for Atmospheric Research (NCAR) Advanced Study Program (ASP) Postdoctoral Fellowship. At NCAR, he worked with the Earth Observing Laboratory (EOL) division developing airborne technology for two-dimensional, electronically scanned, dual-pol phased array radars for atmospheric research. In July 2014, he joined the Advanced Radar Research Center (ARRC), The University of Oklahoma, as a Research Scientist, and became an Assistant Professor with the School of Electrical and Computer Engineering, in August 2015. His research interests include high-performance, broadband antennas for dual-polarized phased array radar applications, array antenna architecture for reconfigurable radar systems, APAA, Tx/Rx modules, radome EM modeling, and millimiter-wave antennas. In 2019, he was awarded the prestigious William H. Barkow Presidential Professorship from The University of Oklahoma, for meeting the highest standards of excellence in scholarship and teaching. He is a Senior Member of the IEEE Antennas and Propagation Society (AP-S), and a Reviewer of various IEEE and AMS conferences and journals.

NAFATI ABOSERWAL (Member, IEEE) received the B.S. degree in electrical engineering from Al-Mergheb University, Alkhoms, Libya, in 2002, and the M.S. and Ph.D. degrees in electrical engineering from Arizona State University, Tempe, AZ, USA, in 2012 and 2014, respectively. In January 2015, he joined the Advanced Radar Research Center (ARRC) and the Department of Electrical and Computer Engineering, The University of Oklahoma (OU), Norman, OK, USA, as a Postdoctoral Research Scientist. He is currently a Research Associate and the Manager of Far-Field, Near-Field and Environmental Anechoic Chambers, Radar Innovations Laboratory (RIL). His research interests include EM theory, computational electromagnetics, antennas, diffraction theory, edge diffraction, and discontinuities impact on the array performance. His research also focuses on active high-performance phased array antennas for weather radars, higher modes and surface waves characteristics of printed antennas, and high-performance dual-polarized microstrip antenna elements with low cross-polarization. He is a member of the IEEE Antennas and Propagation Society (AP-S).